

Fig. 1.— The QSO J2233–606 flux calibrated spectrum smoothed over 2 \AA . Overplotted is the spectrum of the noise per pixel. The emission lines correspond to the SiIV doublet ($\sim 4400 \text{ \AA}$), CIV doublet ($\sim 5000 \text{ \AA}$) and AlIII+ClII] lines ($\sim 6200 \text{ \AA}$). Ticks indicate absorption lines identified in the spectrum. The features around 6850 \AA and 7600 \AA are due to atmospheric absorptions of water vapor.

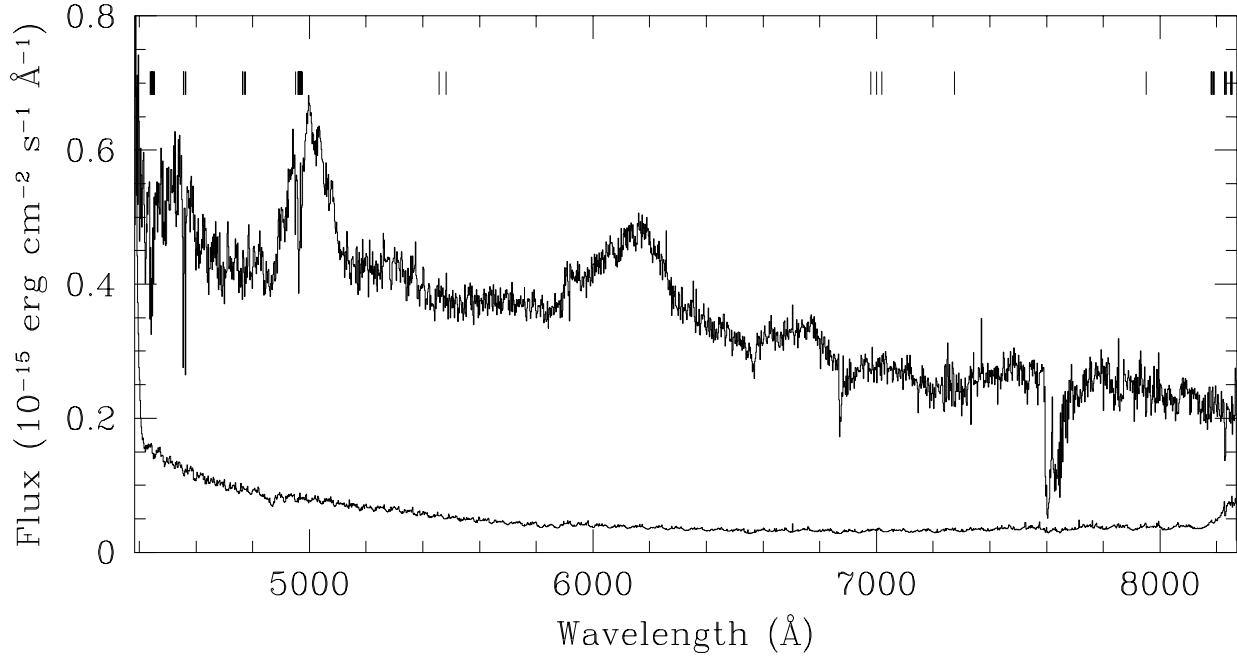


Fig. 2.— The MgII absorption of the metal system at $z = 1.5034$. The thin line is the result of the fit. Also shown is the noise per pixel.

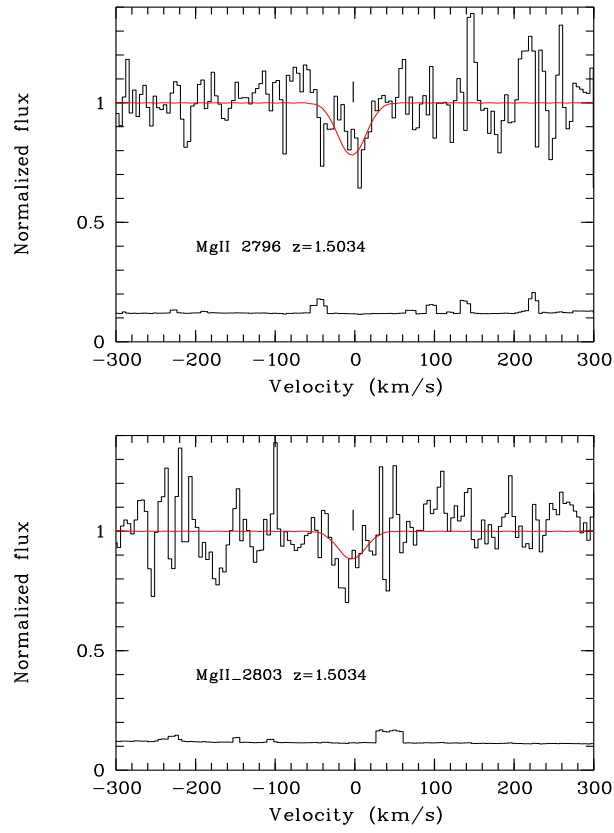


Fig. 3.— As in Fig. 2, but for the CIV absorption of the metal system at $z = 1.7865$.

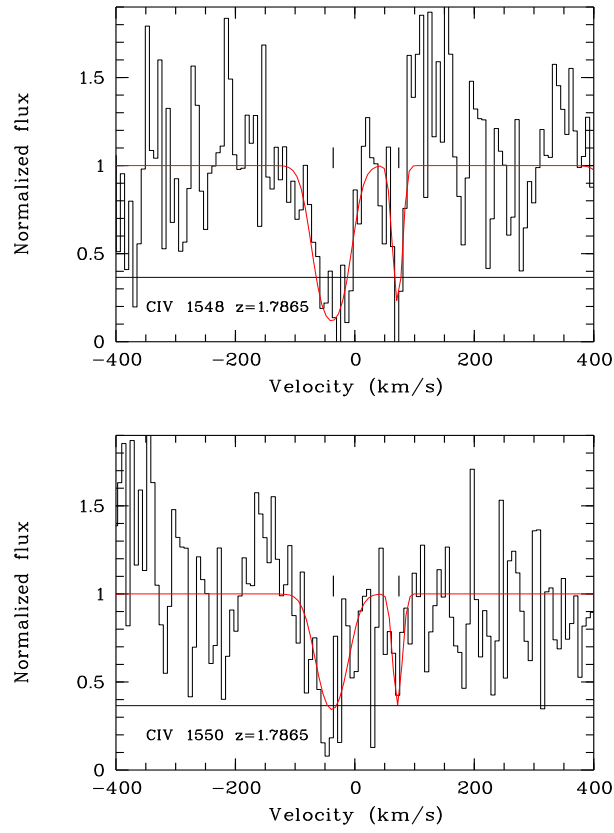


Fig. 4.— As in Fig. 2, but for the CIV and the MgI absorption lines of the metal system at $z = 1.869$.

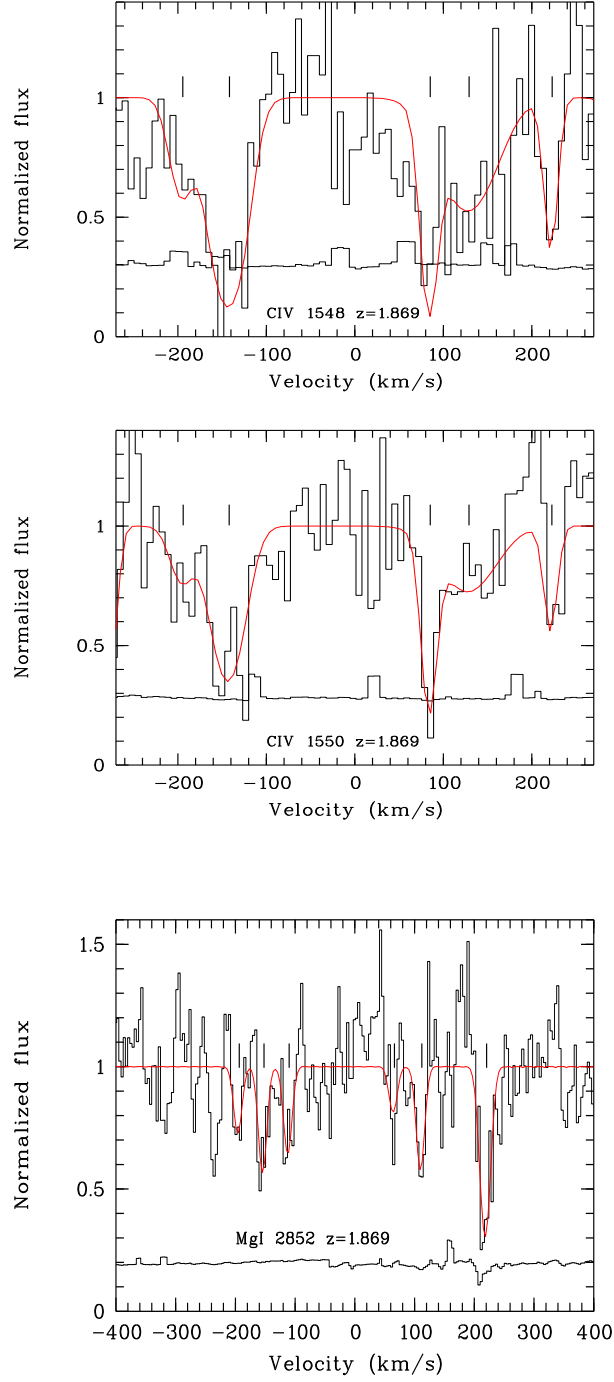


Fig. 5.— As in Fig. 2, but for the CIV and MgII doublets of the metal system at $z = 1.943$.

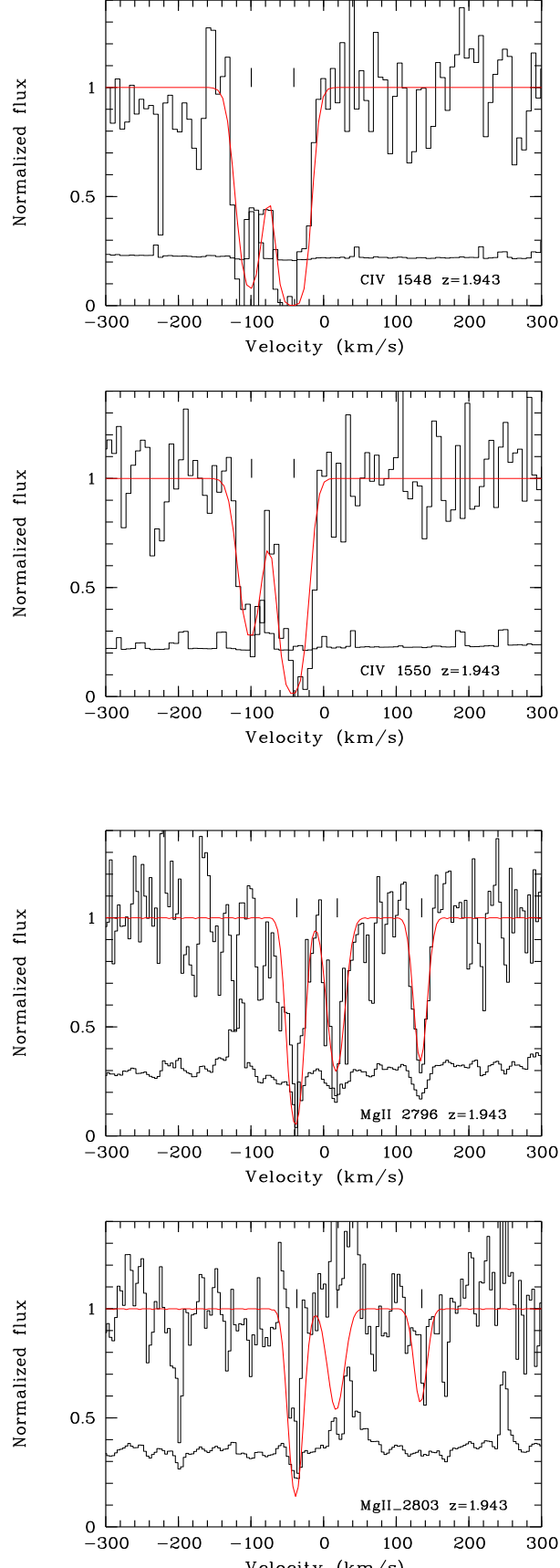


Fig. 6.— As in Fig. 2, but for the CIV doublet of the metal system at $z = 2.077$.

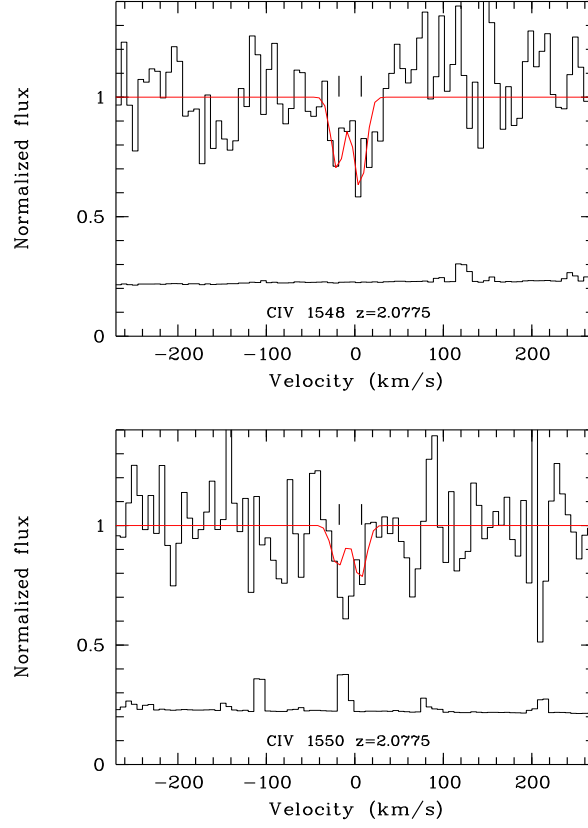


Fig. 7.— The QSO CIV emission peak. Also shown is the spectrum of the noise per pixel.

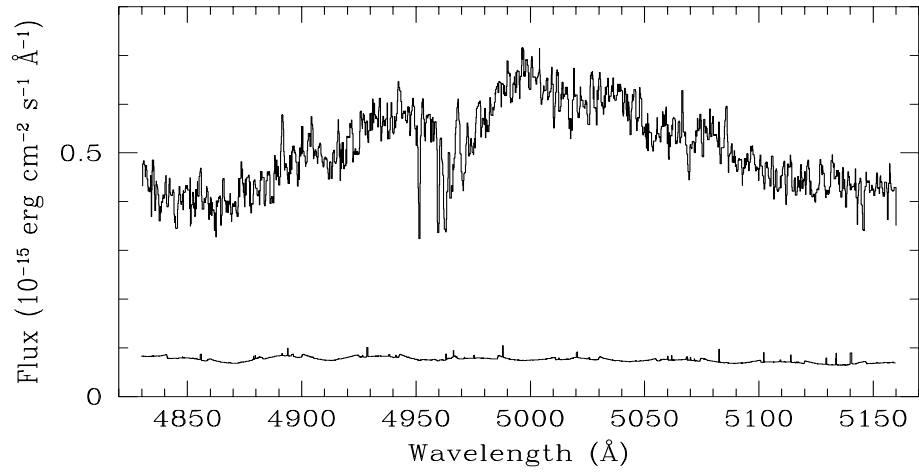


Fig. 8.— Column density ratios in associated systems collected from the literature (Table 8). The straight lines divide the area of non-detection in case of observational limits for CIV, SiIV and NV of $\log N_{CIV} = 12.5$, $\log N_{NV} = 12.1$ and $\log N_{SiIV} = 12.1$ respectively.

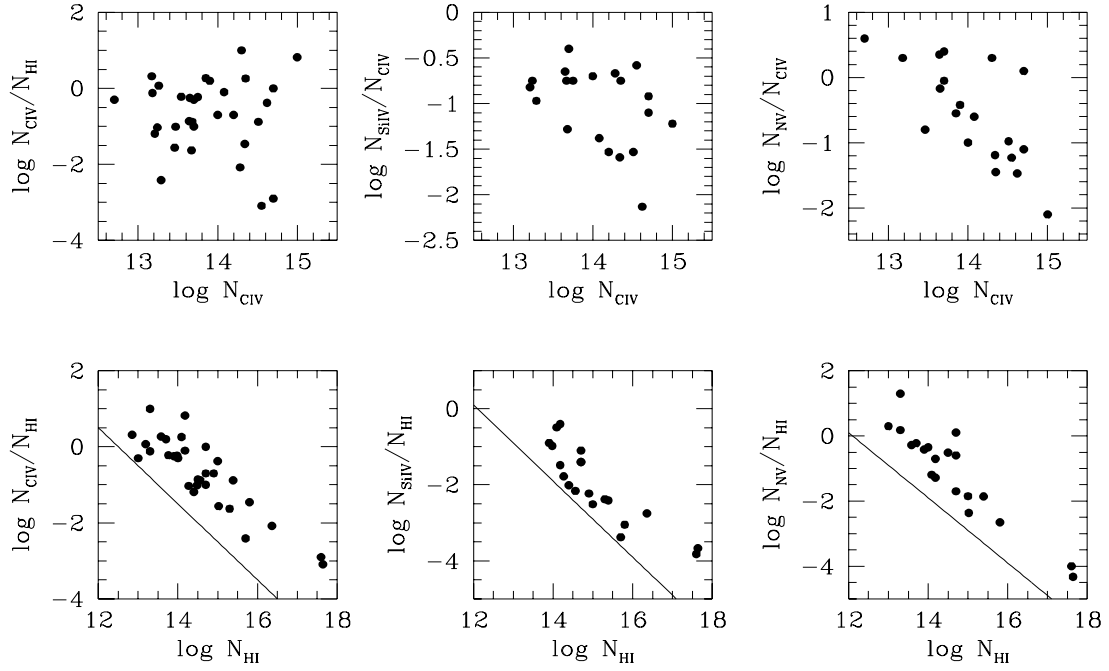


Fig. 9.— As in Fig. 2, but for the CIV complex of the metal system at $z = 2.1982$.

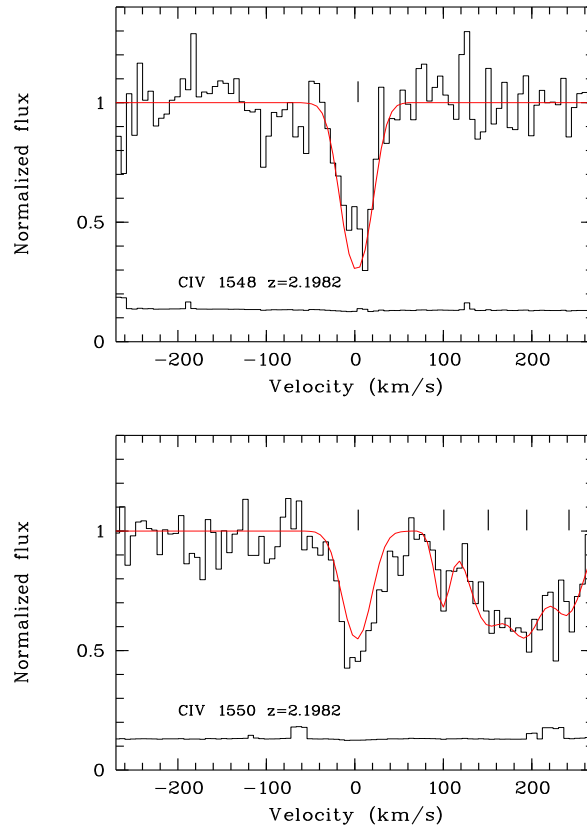


Fig. 10.— As in Fig. 2, but for the CIV complex of the metal system at $z = 2.206$.

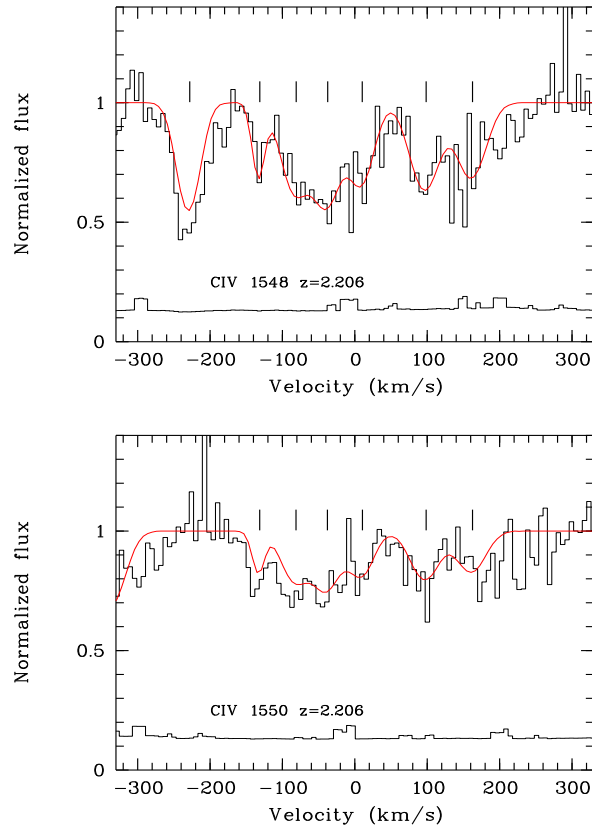
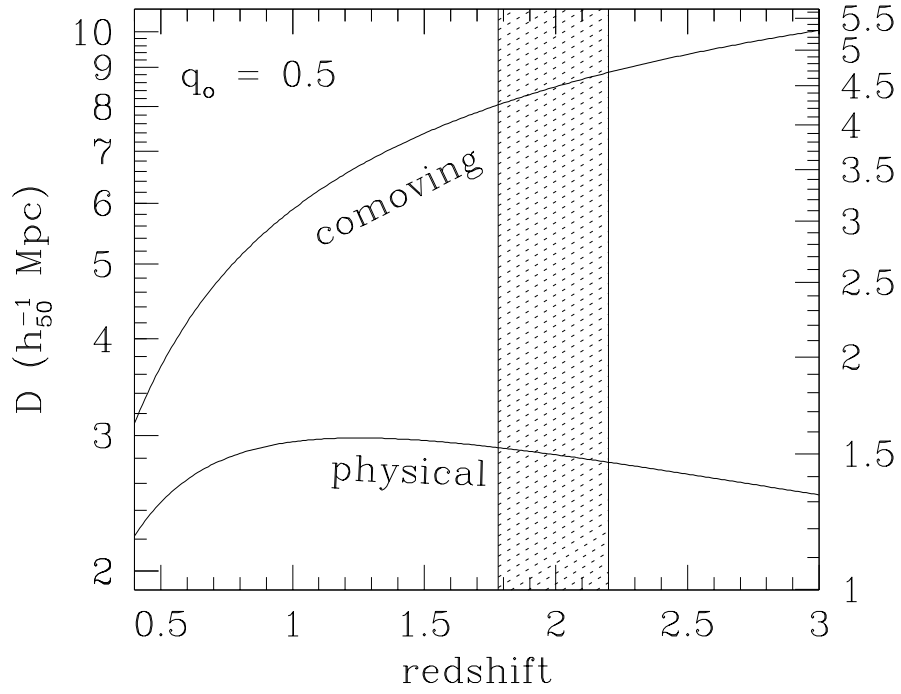


Fig. 11.— Physical and comoving distances as a function of redshift corresponding to angular separations of 5.1 arcmin (left vertical axis) and 2.7 arcmin (right vertical axis). The first is the distance of J2233–606 from the HDFS center, the second is the angular size of the HDFS. The shaded area indicates the redshift range of the identified CIV systems in the QSO spectrum.



THE METAL ABSORPTION SYSTEMS OF THE HUBBLE DEEP FIELD SOUTH QSO

Sandra Savaglio¹

European Southern Observatory, Karl-Schwarzschildstr. 2, D-85748 Garching bei München, Germany

ABSTRACT

The Hubble Deep Field South (HDFS) has been recently selected and the observations are planned for October 1998. We present a high resolution (FWHM $\simeq 14 \text{ km s}^{-1}$) spectrum of the quasar J2233–606 ($z_{em} \simeq 2.22$) which is located 5.1 arcmin East of the HDFS. The spectrum obtained with the New Technology Telescope redward of the Lyman- α emission line covers the spectral range 4386–8270 Å. This range corresponds to redshift intervals for CIV and MgII intervening systems of $z = 1.83 - 2.25$ and $z = 0.57 - 1.95$ respectively. The data reveal the presence of two complex intervening CIV systems at redshift $z = 1.869$ and $z = 1.943$ and two complex associated ($z_{abs} \approx z_{em}$) systems. Other two CIV systems at $z = 1.7865$ and $z = 2.077$, suggested by the presence of strong Lyman- α lines in low resolution ground based and Hubble Space Telescope (HST) STIS observations (Sealey et al. 1998) have been identified. The system at $z = 1.943$ is also responsible for the Lyman limit absorption seen in the HST/STIS spectrum. The main goal of the present work is to provide astronomers interested in the Hubble Deep Field South program with information related to absorbing structures at high redshift, which are distributed along the nearby QSO line of sight. For this purpose, the reduced spectrum, obtained from three hours of integration time, has been released to the astronomical community.

Subject headings: cosmology: observations – quasars: absorption lines – quasars: individual: J2233–606

¹Present address: Space Telescope Science Institute, 3700 San Martin Drive, Baltimore, MD21218, USA.

²Based on observations collected at the European Southern Observatory, La Silla, Chile (ESO Nr. 60.B-0381).

1. INTRODUCTION

The Hubble Deep Field (HDF) program (Williams et al. 1996), which was carried out with the Hubble Space Telescope (HST) in December 1995 in the four filters *UBVI* to the deepest ever reached limiting magnitude, together with followup observations in other spectral bands, can be considered as one of the major astronomical events of the nineties. More than 40 articles on this program have been published in refereed journals between April 1996 and December 1997, confirming the tremendous impact of the observations. Articles related to the high redshift Universe ($z \gtrsim 1$) treat such subjects as the galaxy redshift distribution (Gwyn & Hartwick 1996, Seidel et al. 1996, Lanzetta et al. 1996, Lowenthal et al. 1997), the Global Star Formation History (Madau et al. 1996, Connolly et al. 1997, Guzman et al. 1997) and the clustering properties of galaxies (Colley et al. 1996, Villumsen et al. 1997).

After two years, the Hubble Deep Field South (HDFS) has been planned for Cycle 7 of the HST (Williams et al. 1997, see also the HDF–South Web site at the URL <http://www.stsci.edu/ftp/science/hdf/hdfsouth/hdfs.html>), and the observations will be performed in October 1998. Around the selected Southern field only one high redshift quasar J2233–606 ($z_{em} \simeq 2.22$) has been identified (Boyle 1997),

and it is located 5.1 arcmin EAST of the HDFS. Two HST orbits have been dedicated to this object to obtain a low resolution STIS spectrum (3700 seconds with G230L and 2200 seconds with G430L). The spectrum in the range $\lambda\lambda = 1600 - 5700 \text{ \AA}$ reveals, among other features, the presence of a Lyman limit break at $z \sim 1.9$, a few metal lines in the red part of the Ly α emission line and a Ly α forest with a few absorption lines on the top of the Ly α emission lines. No Damped Ly α profile is seen along the line of sight. Ground–based low resolution observations combined with the STIS spectrum have been analyzed by Sealey et al. (1998). They report a first tentative identification of metal lines and provide a HI column density of the Lyman limit system at $z = 1.943$, of $N(\text{HI}) = (3.1 \pm 1.0) \times 10^{17} \text{ cm}^{-2}$.

Here we report high spectral resolution ($\text{FWHM} \simeq 14 \text{ km s}^{-1}$) observations obtained with the New Technology Telescope (NTT) of the nearby QSO J2233–606 ($z_{em} \simeq 2.22$) in the spectral range $\lambda\lambda = 4386 - 8270 \text{ \AA}$. Even though the 3 hours of integration time have not produced an extremely high quality spectrum, the reduced data have been released to the astronomical community (see the URL <http://www.eso.org/~ssavagli>). It is hoped that these data will provide a valuable guide when planning HDFS followup observations and will assist scientific discussions on the relation between the absorption systems along the QSO line of sight and the emitting objects which will be identified in the HDFS. Other high resolution observations from the ground primarily covering the Lyman– α forest region have been scheduled for July 1998 at the high resolution spectrograph UCLES of the Anglo

Australian Telescope (AAT).

2. THE DATA

The spectrum of the quasar J2233–606 ($z_{em} \simeq 2.22$) has been observed in October 1997 at the ESO 3.5m NTT with the high resolution spectrograph EMMI in the spectral range $\lambda\lambda = 4386 - 8270 \text{ \AA}$. The log of the three exposures of one hour duration each is reported in Table 1. The flux calibration has been done using the spectrum of the standard star HR778 (Hamuy et al. 1992) and the flux has turned out to be about 20% lower than what was found in the HST/STIS spectrum due to slit losses. The echelle mode of EMMI can be used only in the red arm, which does not perform at the highest quality in the blue, where the interesting part of the spectrum is, between the Ly α and the CIV emission lines ($\lambda\lambda = 3940 - 5020 \text{ \AA}$). To avoid overlapping of the orders in the blue part of the CCD, we limited the slit length to 4 arcsec, which created some problems for sky subtraction.

Vacuum and heliocentric wavelength calibration obtained using the Thorium–Argon lamp, gave an accuracy of the order of less than one tenth of a pixel. The final combined spectrum has been rebinned to a constant pixel size of 0.1 \AA . The spectral resolution measured from the lamp emission lines is $\text{FWHM} \simeq 11 \text{ km s}^{-1}$, but the real resolution in the final spectrum is somewhat degraded due to the merging of the three spectra and to a possible slight drift of the object in the slit during the exposure. The final assumed resolution is that measured from the sky emission lines, and that is $\text{FWHM} \simeq 14 \text{ km s}^{-1}$.

Observations were complicated by the low position of the object ($\delta = -60^\circ 33'$) in the sky of la Silla ($\delta = -29^\circ 15'$) and by its visibility. At the end of October the object was at the meridian just at the beginning of the night. The airmass ranged from 1.2 at the start to 1.5 at the end of the observations. The seeing monitor station located at La Silla Observatory registered during the exposures a seeing varying from 0.9 arcsec to 1.5 arcsec, with an average around 1.1 arcsec. However that should be considered as a lower limit, since the seeing at the telescope is normally higher than that measured outside the dome.

Fig. 1 shows the entire spectrum in the spectral range $\lambda\lambda = 4386 - 8270 \text{ \AA}$ degraded to low resolution. The spectrum data reduction – carried out with the MIDAS software package ECHELLE – has been done together with the spectrum of the noise, which is important for the determination the significance of absorption lines in the spectrum. That has been calculated from the propagation of the photon statistics of the object and sky spectra and from the detector read-out-noise. The redshift of the QSO can be estimated from the CIV emission line, in spite of the absorption complex close to the emission peak and

the asymmetric profile of the line that complicate the fit. The peak is probably in the range $\lambda = 4980 - 5000 \text{ \AA}$ which gives $z_{em} \simeq 2.22$, although as shown by Espey (1993) the best estimate of the actual redshift is given by the low ionization lines, such as the MgII doublet. The obtained redshift is somewhat lower than that found by low resolution observations (Sealey et al. 1998), which give $z_{em} = 2.238$ from the fit of several emission lines.

The MIDAS package FITLYMAN (Fontana & Ballester 1995) has been used to measure the parameters of absorption lines. Line fitting through χ^2 minimization of Voigt profiles has been performed, although complex features commonly seen in metal systems are difficult to resolve in this spectrum due to the limited signal-to-noise ratio. The number of components is normally underestimated due to blending. This means that the fit of a blended profile gives a Doppler parameter b which is not particularly significant, whereas the column density corresponds, to a good approximation, to the total column density of individual real lines.

3. THE METAL SYSTEMS OF J2233–606

To identify metal lines in a quasar spectrum, the first approach is to look for double features and to compare wavelengths with the most common and strong doublets typically observed, namely CIV, SiIV and redshifts MgII. Then isolated lines can be identified if associated with the discovered systems. The data presented here cover the CIV, SiIV, MgII absorptions for intervening systems in the redshift range $z = 1.83 - 2.25$, $z = 2.15 - 2.25$, $z = 0.57 - 1.95$ respectively.

The spectrum of J2233–606, observed at low resolution with HST/STIS and from the ground with the Australian National University (ANU) 2.3m telescope (Sealey et al. 1998), shows a Lyman limit absorption around 2700 \AA ($z \simeq 1.94$) with HI column density $N(\text{HI}) = (3.1 \pm 1.0) \times 10^{17} \text{ cm}^{-2}$ and a few metal absorption lines redward of the Ly α emission line identified as possible CIV absorptions. The high resolution observations presented here, allowed us to identify the strong CIV doublets, which were seen as single lines in the STIS and ANU spectra. Given the redshift of these systems, we have attempted the identification of other absorption lines in the spectral range associated with every single CIV system found. We report some detections and in many cases upper limits on ion column densities.

Tables 2–7 list the results of fitting procedures for the intervening systems. These are three strong CIV systems at $z = 1.7865$, $z = 1.869$ and $z = 1.943$ and one weak CIV system at $z = 2.077$. One possible MgII system candidate at $z = 1.5034$ has been reported, although it does not show any strong Lyman- α at the same redshift. We also discuss the system at $z = 1.928$ reported by Sealey et al. (1998), for which we do not find strong absorption lines.

In Tables 9 and 10 we present results for the associated systems ($z_{abs} \approx z_{em}$) at $z = 2.198$ and $z = 2.206$ identified through the detection of CIV absorption. The tables are organized as follows: the reported are relative to the CIV doublet, or the MgII doublet when CIV is not detected (i.e. for the system at $z = 1.5034$ and for the last two components of the $z = 1.943$ complex system). When an ion has not been detected in the spectrum, we report only an upper limit to the column density for a given Doppler parameter b which typically gives a χ^2 for the residuals of the fit around 2 or larger. In these cases the adopted Doppler parameter is reported in parenthesis. This is in the range $20 - 30 \text{ km s}^{-1}$, considerably higher than that typically observed in metal absorption lines, which should give conservative column density upper limits. In a few cases the detected line is given with the Doppler parameter reported in parenthesis as well, indicating that b has been assumed rather than obtained (in cases in which the fit has not given a realistic b value).

The following two sections describe the redshift identification of the individual intervening and associated metal systems.

3.1. The intervening systems

In spite of the fact that the observed spectral range covers a wide redshift interval for the MgII absorption ($z = 0.57 - 1.95$), one of the most typical metal doublets observed in QSO spectra, only one strong MgII doublet has been identified, at $z = 1.943$. The observational limit for the column density of this doublet varies along the spectrum and for a Doppler parameter of 20 km s^{-1} is $\log N(\text{MgII}) \simeq 13.1$ around 4700 \AA , 12.7 around 5500 \AA , 12.5 around 6200 \AA where the S/N is maximum, 12.6 around 7000 \AA and 12.9 around 7900 \AA . The SiIV coverage is very limited with no detection. The CIV range extends from $\sim 4400 \text{ \AA}$ to the emission line at $\sim 5000 \text{ \AA}$.

3.1.1. The metal system at $z = 1.5034$

We report this system through a tentative identification of a weak MgII doublet at $\sim 7000 \text{ \AA}$ (Fig. 2) and it needs further observations to be confirmed. No other lines have been detected (Table 2). If this metal system were real, it should have shown a strong Ly α absorption line at 3043 \AA which does not appear in the STIS data. The closest strong feature seen is around 3000 \AA , which would correspond, in the case of a Ly α line, to a redshift of $z \simeq 1.47$, that is 4000 km s^{-1} blueward of this MgII doublet.

3.1.2. *The metal system at $z = 1.7865$*

Sealey et al. (1998) report a possible metal system at redshift $z = 1.787$ associated with a prominent Ly α line seen in the STIS spectrum and perhaps with a CIV doublet. The associated CIV doublet would be at $\lambda \simeq 4320$ Å. At that spectral interval, our EMMI data have very little signal, and for this reason we have excluded at first that part of the CCD from the data reduction. Subsequently, we dedicated particular attention to this interval, in an attempt to detect the CIV absorption. In Fig. 3 we show the two components found, which give a total CIV column density $\log N(\text{CIV}) \simeq 14.3$ (Table 3).

At $\lambda \simeq 7951.5$ Å there is an absorption line that corresponds to the MgI $\lambda\lambda 2852$ line of the second component of this system and that looks like a complex structure. We have fitted it with one line at $z = 1.787115$. The MgI associated with the first, stronger CIV component is not detected.

3.1.3. *The metal system at $z = 1.869$*

This metal system shows a complex CIV absorption (Fig. 4) and only a much higher S/N in the spectrum could make it possible to deblend the lines. We have fitted 5 components, but there could be more. The total CIV column density is $N(\text{CIV}) \simeq 3 \times 10^{14} \text{ cm}^{-2}$ with a large uncertainty due to the uncertainties on the individual components (Table 4). Besides the CIV complex structure, we identified the MgI $\lambda\lambda 2852$ lines at $\lambda \simeq 8185$ Å (Fig. 4). The second CIV component (at $z = 1.867628$) shows a double MgI feature for which we report only the total column density (in this case $b = 5 \text{ km s}^{-1}$ is assumed for both absorptions).

The presence of low ionization species like MgI is typical for high HI density clouds, e.g. in damped Ly α systems. For a Lyman limit system with $\log N(\text{HI}) \sim 17$, the MgI column density should be much lower than our detection limit (for a metallicity of 1/100 of solar) and at least 2 orders of magnitude lower than the MgII column density. If the MgI identification were real, we should have also detected the MgII doublet. This consideration makes the MgI detection in this system suspicious. The other explored possibility is that the complex absorption at $\lambda \simeq 8185$ Å corresponds to the MgII $\lambda\lambda 2796$ lines of the system at $z = 1.928$, that Sealey et al. (1998) identified as a possible contributor to the Lyman limit break. In the following paragraph we argue that this solution is also not satisfactory, making the identification of the absorption lines seen at $\lambda \simeq 8185$ Å still doubtful.

The spectrum shows at $\lambda = 6722.2$ Å an absorption line which would correspond to the FeII $\lambda\lambda 2344$ feature at $z = 1.8676$, but the fit – with all the 6 lines of the FeII ion in the spectral range – rules out this identification.

3.1.4. *A possible metal system at $z = 1.928$*

Although Sealey et al. investigate this system as a candidate contributor to the observed Lyman break at $\lambda \simeq 2700 \text{ \AA}$, they in fact conclude that this is probably dominated by the system at $z = 1.943$. Table 5 gives the column density due to the identification of the $\lambda\lambda 2484$ line, and the FeII column density due to the identification of the FeII $\lambda\lambda 2382$ line. Both of these lines are very weak and their detection needs further confirmation. No associated CIV has been found and the upper limit to the column density is $\log N(\text{CIV}) < 13.7$. Another possible detection would be the MgII $\lambda\lambda 2796$ at $\lambda \simeq 8185 \text{ \AA}$, but we consider the identification unlikely since the second component of the doublet MgII $\lambda\lambda 2803$ is not detected.

3.1.5. *The metal system at $z = 1.943$*

This system is the main contributor to the Lyman break seen in the STIS spectrum at 2700 \AA ($\log N(\text{HI}) \simeq 17.5$). It is probably associated with multi-phase gas clouds since it shows a strong CIV doublet with a double structure and a MgII doublet with a triple structure by $100 - 200 \text{ km s}^{-1}$ (Fig. 5). The S/N is not high enough to resolve a higher number of components which are often seen in strong CIV systems. The results of the fitting procedures are shown in Table 6. The first CIV component at $z = 1.942007$ is not saturated and it gives a reasonable result for $\log N(\text{CIV}) \simeq 14.1$. The second at $z = 1.942582$ is saturated with a higher uncertainty on the fitted parameters. The total CIV column density is $\log N(\text{CIV}) = 14.7 \pm 0.5$. The MgII column density might indicate a high metallicity compared with that found in typical Lyman limit systems (in the range between 1/100 and 1/30 of solar, Steidel 1990). That would be confirmed by the detected AlIII ion in the second component of the system, but not by the low upper limit found for the column density of the AlIII ion.

There is a double feature corresponding to CI at $z = 1.943607$ and $z = 1.944033$ at $\lambda \simeq 4594 \text{ \AA}$ which could be associated with the two reddest MgII components. Unfortunately the signal in the spectrum is very low and the identification is doubtful.

3.1.6. *The metal system at $z = 2.077$*

This metal system shows a very weak CIV doublet and that is the only detected metal ion, whereas the STIS spectrum shows a strong Ly α line at the same redshift. The CIV $\lambda\lambda 1550$ line falls very close to a noisy peak making the detection of this system more complicated. The CIV fit requires at least two components. The results are given in Table

7 and shown in Fig. 6 assuming $b = 5 \text{ km s}^{-1}$ for both the components. The observed total CIV column density of a few 10^{13} cm^{-2} could give an HI column density absorption around 10^{15} cm^{-2} for a cloud with a metallicity of 1/100 of solar, photoionized by a UV background QSO dominated with a softness parameter $S_L \equiv J_{912}/J_{228} \sim 100^3$ and absorbed by the Intergalactic Medium.

3.2. The associated systems

The STIS spectrum of J2233–606 shows several absorption lines around the peak of the $\text{Ly}\alpha$ emission line, some of which are $\text{Ly}\alpha$ lines with CIV absorption. Fig. 7 shows a portion of the EMMI spectrum smoothed over 9 pixels around the CIV emission peak (at $z \simeq 2.22$) in the redshift range $\pm 5000 \text{ km s}^{-1}$. A cluster of CIV lines is clearly seen around 4960 \AA . Other spurious features are visible, but no other CIV doublets have been identified, although they are probably present.

Associated absorption systems ($z_{\text{abs}} \approx z_{\text{em}}$) have caught the astronomers’ interest since they give the opportunity to explore the physical conditions of high redshift absorbing gas clouds. It is not clear yet whether these clouds are associated with the quasar itself, have their origin in the Interstellar Medium of the hosting objects or are located somewhere in the cluster which contains the quasar. It has been shown (Savaglio et al. 1994, Møller et al. 1994, Petitjean et al. 1994, Savaglio et al. 1997, Hamann et al. 1997) that the gas in these clouds is metal rich already by redshift $z \sim 4$, indicating a strong stellar activity in the environment, also confirmed by an overabundance of α -elements. To compare the properties of the prominent associated absorption systems in J2233–606 with what is known so far, we collected high resolution data from the literature (Table 8) and plotted them in Fig. 8.

Tables 9 and 10 list column densities for the systems found in J2233–606. They basically contain CIV detections and upper limits for other ions. For completeness we also report results for low ionization species which fall in the observed range even if they are typically not detected in the associated systems.

³The softness parameter S_L is defined as the ratio of the intensities of the UV background J_ν at the HI and HeII Lyman limit, at 912 \AA and 228 \AA respectively.

3.2.1. *The metal system at $z = 2.1982$*

This associated system (Table 9) shows a strong CIV doublet at about -2000 km s^{-1} from the emission peak. The fit with one component gives a relatively poor result since the equivalent width ratio of the first line CIV $\lambda\lambda$ 1548 relative to the second CIV $\lambda\lambda$ 1550 is lower than expected (Fig. 9). A fit with a double structure does not result in a better fit. There may be two possible explanations for this discrepancy: either the second line is contaminated by another unidentified absorption line or the level of the continuum has been underestimated for the first line and/or overestimated for the second. However, we consider it unlikely that the second possibility would affect the fit so much.

Other strong doublets typically seen in associated systems are NV and SiIV. The ratio of the SiIV to CIV column densities is typically spread over a wide range (Fig. 8) and the upper bound of the distribution is $\log[N(\text{SiIV})/N(\text{CIV})] \approx -0.5$, which would give for this system – with $\log N(\text{CIV}) \simeq 13.8$ – an upper limit to the SiIV column density of $\log N(\text{SiIV}) \lesssim 13.3$, just at the level of our detection limit. Other high or intermediate ionization species are out of our spectral range. From the correlation seen in the $\log[N(\text{NV})/N(\text{CIV})]$ vs. $\log N(\text{CIV})$ plot (Fig. 8), we expect for the NV column density at $\lambda \simeq 3966 \text{ \AA}$ a value which is $\log N(\text{NV}) \approx 13.4$. Concerning the HI column density, the bulk of the associated systems around the observed CIV column density of $\log N(\text{CIV}) \simeq 13.8$ is $-1.0 < \log[N(\text{CIV})/N(\text{HI})] < 0.1$ (Fig. 8), which means that we could expect a HI column density in the range $13.7 \lesssim \log N(\text{HI}) \lesssim 14.8$.

3.2.2. *The metal system at $z = 2.2058$*

This system shows a multiple component CIV absorption in the redshift range between about -1400 km s^{-1} and -1100 km s^{-1} from the emission peak (Fig. 10). The fitting procedures are very complicated due to a probable intrinsic blending of the lines and to the low S/N. The number of components is then very uncertain. In Table 10 we report the results for a structure with 6 components for a total CIV column density around 10^{15} cm^{-2} . Upper limits to the SiIV column density are not particularly significant. Given the CIV column density of individual components, the associated HI column densities are most likely lower than 10^{15} cm^{-2} , while NV could be detected with column density $\log N(\text{NV}) \approx 13$.

4. DISCUSSION

Unlike in the case of the HDF North program, “follow-up” observations of the HDFs region from the ground and space telescopes began already long before the beginning of the program. The observations from the radio to X-rays, from low and high resolution spectroscopy to narrow and broad band imaging, programmed since November 1997 to the Spring of 1999, will be combined to provide astronomers with the deepest and most complete view of the Universe for redshifts $z > 1$, where most of the stars have probably already formed.

Moreover, unlike the Northern field, the HDFs is close to a high redshift quasar. The QSO line of sight ($\alpha = 22^h33'37.67''$, $\delta = -60^\circ33'28.95''$, J2000 Equinox) is located $5'7''$ away from the Hubble Deep Field South ($\alpha = 22^h32'56.22''$, $\delta = -60^\circ33'02.69''$, J2000 Equinox). This corresponds to a real separation that is shown in Fig. 11 in the redshift range $z = 0.5-3$. The separation at the QSO redshift ($z_{em} \simeq 2.22$) is 2.8 and 8.9 h_{50}^{-1} Mpc (h_{50} is the Hubble constant expressed in units of $50 \text{ km s}^{-1} \text{ Mpc}^{-1}$) for a flat Universe in the physical and comoving space respectively.

Deep imaging of the region near the QSO line of sight is fundamental to the understanding the quasar environment, the origin of high redshift quasars in connection to that of galaxy clusters and the relation between Ly α absorbers and high redshift galaxies. The typical wavelength of density fluctuations whose collapse generate galaxy clusters is around $20 h_{50}^{-1}$ Mpc. On the other hand, once virialized, clusters have a typical size (i.e., virial radius) of about $2-5 h_{50}^{-1}$ Mpc, depending on their mass and on the background cosmological model (e.g., Kitayama & Suto 1996, and references therein). At redshift $z \sim 2.2$ we generally expect to find protoclusters which are not yet virialized. Instead, they should correspond to detectable overdensities involving scales of about $10 h_{50}^{-1}$ Mpc comoving. Therefore, that would roughly correspond to the comoving separation between the HDFs and the main absorption clusters seen in the QSO spectrum, whereas at the same redshift, the comoving HDFs size is around $4.5 h_{50}^{-1}$ Mpc. The size of the HDFs and the separation from the quasar might be suitable for the identification of clustered structures associated with the QSO absorption systems.

The idea of the existence of clustered structures at high redshifts has recently been confirmed by observations. Steidel et al. (1998) found evidence for a protocluster of galaxies at $z \simeq 3.1$ in the field of two high redshift QSOs, one of which is at the same redshift as the structure. The discovered 15 Lyman break galaxies are distributed on a plane which is at least $20 \times 15 h_{50}^{-2} \text{ Mpc}^2$ comoving. Numerical simulations have shown that non-linear structures can be present on large scales already by $z = 3$. Using N-body simulations and semi-analytical methods, Governato et al. (1998) were able to produce in the generic Cold

Dark Matter scenario, structures similar to the observed one. These high redshift associations of Lyman break galaxies are strongly biased with respect to the already overdense local dark matter distribution and are the seeds of present day galaxy clusters.

Other protoclusters of galaxies candidates at very high redshift ($z \sim 2$) have been found in a limited number of cases (Dressler et al. 1993, Francis et al. 1996, Pascarelle 1996, Hutchings 1995). At low redshift ($z < 1$) extensive imaging and spectroscopic observations of galaxy clusters in quasar environments and other AGNs indicated that quasar activity is strongly correlated with the properties of the environment of the host galaxy (Yee & Green, 1987; Yee & Ellingson, 1993). The study of the HDFS QSO should allow to extend this concept to much higher redshifts. In particular, it should reveal if the highest density peaks that give origin to quasars at high redshift are also the seeds of structure formation on much larger scales.

5. SUMMARY

We provide the first results of high spectral resolution observations of the quasar J2233–606 which lies close to the selected Hubble Deep Field South. The main motivation for this work is to give the astronomical community interested in the HDFS access to information on collapsed structures along the QSO line of sight. The spectrum shows two strong CIV systems, at $z = 1.869$ and $z = 1.942$, the latter being also responsible for the Lyman limit absorption seen in the HST/STIS spectrum. Also detected are two strong associated systems ($z_{abs} \approx z_{em} \approx 2.2$) with prominent CIV absorption. Moreover, we have confirmed the presence of two other less certain CIV systems at $z = 1.7865$ and $z = 2.077$, suggested by the analysis of the HST/STIS spectrum. Finally one tentative MgII detection at $z = 1.5034$ needs further observations for confirmation. Despite the limited integration time, we have been able to perform fitting procedures to the data and derive column density measurements and upper limits for all the ions in the observed range. This information can be combined with high resolution observations of the Ly α forest planned for July 1998 at the AAT/UCLES, in order to derive the ionization state and the heavy element enrichment of the identified systems. The ultimate goal of this study would be to understand the origin and the evolution of the high redshift structures which will be detected in the Hubble Deep Field South.

It is my pleasure to thank Stefano Borgani, Adriano Fontana, Mario Livio, Nino Panagia and John Webb for useful discussions. I am also grateful to Sandro D’Odorico and Emanuele Giallongo for support with the observations. My special acknowledgment goes to the HDFS

team, in particular to Massimo Stiavelli for inspiring this work and to Marcella Carollo and Harry Ferguson for reducing the STIS data and making them available.

REFERENCES

- Boyle B. J., 1997, AAO Newsletter, 83, 4
- Dressler A., Oemker A., Gunn J. E., Butcher H., 1993, ApJ, 404, L45
- Espey B. R., 1993, ApJ, 411, L59
- Fan X–M., Tytler D., 1994, ApJS, 94, 17
- Fontana A., Ballester P., 1995, *The ESO Messenger*, 80, 37
- Francis P. J., Woodgate B. E., Warren S. J., et al., 1996, ApJ, 457, 490
- Governato F., Baugh C. M., Frenk, C. S., Cole S., Lacey C. G., Quinn T., Stadel J., 1998, Nat, 392, 359
- Guzman R., Gallego J., Koo D. C., et al., 1997, ApJ, 489, 559
- Gwyn S. D. J., Hartwick F. D. A., 1996, ApJ, 468, L77
- Hamann F., Barlow T. A., Junkkarinen V., Burbidge E. M., 1997, ApJ, 478, 80
- Hamuy M., et al., 1992, PASP, 104, 533
- Hutchings J. B., 1995, AJ, 109, 928
- Kitayama T., Suto Y., 1996, ApJ, 469, 480
- Lanzetta K. M., Yahil A., Fernandez–Soto A., 1996, Nat, 381, 759
- Lowenthal J. D., Koo D. C., Guzman R., et al., 1997, ApJ, 481, 673
- Madau P., Ferguson H. C., Dickinson M. E., Giavalisco M., Steidel C. C., Fruchter A., 1996, MNRAS, 283, 138
- Møller P., Jakobsen P., Perryman M. A. C., 1993, A&A, 287, 719
- Pascarelle S. M., Windhorst R. A., Driver S. P., Ostrander E. J., Keel W. C., 1996, ApJ, 456, L21
- Petitjean P., Rauch M., Carswell R. F., 1994, A&A, 291, 29
- Savaglio S., D’Odorico S., Møller P., 1994, A&A, 281, 331

- Savaglio S., Cristiani S., D’Odorico S., Fontana A., Giallongo E., Molaro P., 1997, *A&A*, 318, 347
- Sealey K. M., Drinkwater M. J., Webb J. K., 1998, *ApJL*, *in press*
- Songaila A., Cowie L. L., 1996, *AJ*, 112, 335
- Steidel C. C., 1990, *ApJSS*, 74, 37
- Steidel C. C., Adelberger K. L., Dickinson M., Giavalisco M., Pettini M., Kellogg M., 1998, *ApJ*, 492, 428
- Steidel C. C., Giavalisco M., Dickinson M., Adelberger K. L., *AJ*, 112, 352
- Villumsen J. V., Freudling W., da Costa L. N., 1997, *ApJ*, 481, 578
- Wampler E. J., Bergeron J., Petitjean P., 1993, *A&A*, 273, 15
- Williams R. E., Baum S. A., Blacker B. et al., 1997, *Bull. American Astron. Soc.*, 191, #105.08
- Williams R. E., Blacker B., Dickinson M. et al., 1996, *AJ*, 112, 1335
- Yee, H. K. C., Ellingson, E., 1993, *ApJ*, 411, 43
- Yee, H. K. C., Green, 1987, *ApJ*, 319, 28

Table 1: Log of the observations.

#	date	range (Å)	grating	CD grism	slit width	exposure (s)	mean airmass
1	29/10/97	4386 – 8270	10	#3	1.2''	3600	1.2
2	29/10/97	4386 – 8270	10	#3	1.2''	3600	1.3
3	29/10/97	4386 – 8270	10	#3	1.4''	3600	1.4

Table 2: The metal system at $z = 1.5034$.

Ion	$z = 1.503369$	
	$\log N$	b
SiI	< 13.1	(25)
AlIII	< 12.9	(25)
MgI	< 11.8	(25)
MgII	12.37 ± 0.10	22.7 ± 6.1
FeI	< 12.4	(20)
FeII	< 12.9	(20)

Table 3: The metal system at $z = 1.7865$.

Ion	$z = 1.786142$		$z = 1.787161$	
	$\log N$	b	$\log N$	b
CIV	14.18 ± 0.11	30.1 ± 6.3	13.82 ± 1.10	5.1 ± 5.5
SiI	< 13.3	(20)	< 13.3	(20)
SiII	< 14.6	(20)	< 14.6	(20)
AlII	< 12.5	(20)	< 12.5	(20)
AlIII	< 12.8	(20)	< 12.8	(20)
MgI	< 12.1	(20)	12.31 ± 0.07	26.5 ± 4.3
MgII	< 12.7	(20)	< 12.7	(20)
FeI	< 12.8	(20)	< 12.8	(20)
FeII	< 12.7	(20)	< 12.7	(20)
ZnII	< 12.7	(20)	< 12.7	(20)

Table 4: The metal system at $z = 1.869$.

Ion	$z = 1.867128$		$z = 1.867628$		$z = 1.869800$		$z = 1.870218$		$z = 1.871119$	
	$\log N$	b	$\log N$	b	$\log N$	b	$\log N$	b	$\log N$	b
CI	< 13.9	(20)	< 13.7	(20)	< 13.7	(20)	< 13.7	(20)	< 13.9	(20)
CIV	13.34±0.24	15.9±11.3	14.07±0.10	23.2±5.2	13.98±0.,41	7.3±3.9	13.79±0.16	41.5±21.2	13.49±0.53	5.8±6.5
SiI	< 13.1	(20)	< 13.1	(20)	< 13.1	(20)	< 13.1	(20)	< 13.1	(20)
SiII	< 14.4	(20)	< 13.5	(20)	< 14.0	(20)	< 13.8	(20)	< 14.3	(20)
AlII	< 12.4	(20)	< 12.4	(20)	< 12.4	(20)	< 12.4	(20)	< 12.4	(20)
AlIII	< 12.7	(20)	< 12.6	(20)	< 12.8	(20)	< 12.6	(20)	< 12.6	(20)
MgI*	11.64±0.22	(5)	12.17±0.25**	–	11.44±0.28	(5)	11.91±0.15	(5)	12.31±0.14	8.0±4.0
MgII	< 12.7	(20)	< 12.7	(20)	< 12.7	(20)	< 12.7	(20)	< 12.7	(20)
FeI	< 12.5	(20)	< 12.6	(20)	< 12.5	(20)	< 12.5	(20)	< 12.8	(20)
FeII	< 12.9	(20)	< 13.2	(20)	< 13.0	(20)	< 13.0	(20)	< 12.9	(20)
ZnII	< 12.7	(20)	< 12.7	(20)	< 12.7	(20)	< 12.7	(20)	< 12.7	(20)

* Suspected blend with MgII λ 2796 at $z = 1.928$

** Two components have been fitted assuming for both $b = 5 \text{ km s}^{-1}$.

Table 5: The metal system at $z = 1.928$.

Ion	$z = 1.9288$	
	$\log N$	b
CI	< 13.8	(20)
CIV	< 13.7	(20)
SiI	< 13.2	(20)
SiII	< 13.6	(20)
AlII	< 12.5	(20)
AlIII	< 12.8	(20)
MgI	< 13.3	(20)
MgII	< 12.8	(20)
FeI	12.39 ± 0.10	10.3 ± 4.5
FeII	12.40 ± 0.16	(5)
ZnII	< 12.7	(20)

Table 6: The metal system at $z = 1.943$.

Ion	$z = 1.942007$		$z = 1.942582$		$z = 1.943143$		$z = 1.944293$	
	$\log N$	b	$\log N$	b	$\log N$	b	$\log N$	b
CI	< 13.7	(20)	< 13.7	(20)	13.35 ± 0.27	8.9 ± 10.3	13.34 ± 0.29	14.4 ± 11.2
CIV	14.06 ± 0.11	17.1 ± 2.7	14.61 ± 0.52	16.2 ± 5.1	< 13.4	(20)	< 13.5	(20)
SiI	< 13.3	(20)	< 13.3	(20)	< 13.3	(20)	< 13.3	(20)
SiII	< 13.4	(20)	< 13.4	(20)	< 13.4	(20)	< 13.4	(20)
AlII	< 12.2	(20)	< 12.2	(20)	< 12.2	(20)	< 12.2	(20)
AlIII	< 12.6	(20)	12.10 ± 0.19	5.8 ± 5.8	< 12.6	(20)	< 12.6	(20)
MgI	< 13.1	(20)	< 13.1	(20)	< 13.1	(20)	< 13.1	(20)
MgII	< 12.7	(20)	13.37 ± 0.14	8.8 ± 1.6	12.87 ± 0.09	12.4 ± 4.1	12.74 ± 0.10	8.4 ± 3.0
FeI	< 12.6	(20)	< 12.6	(20)	< 12.7	(20)	< 12.7	(20)
FeII	< 13.0	(20)	< 13.0	(20)	< 13.0	(20)	< 13.0	(20)
ZnII	< 12.6	(20)	< 12.6	(20)	< 12.6	(20)	< 12.6	(20)

Table 7: The metal system at $z = 2.077$.

Ion	$z = 2.077301$		$z = 2.077561$	
	$\log N$	b	$\log N$	b
Cl	< 13.8	(20)	< 13.8	(20)
CIV	12.95 ± 0.25	(5)	13.08 ± 0.20	(5)
SiI	< 12.9	(20)	< 12.9	(20)
SiII	< 13.3	(20)	< 13.3	(20)
AlII	< 12.3	(20)	< 12.3	(20)
AlIII	< 12.6	(20)	< 12.6	(20)
MgI	< 13.4	(20)	< 13.4	(20)
FeI	< 13.0	(20)	< 13.0	(20)
FeII	< 13.0	(20)	< 13.0	(20)
ZnII	< 12.7	(20)	< 12.7	(20)

Table 8: The associated ($z_{abs} \approx z_{em}$) QSO metal systems known from the literature.

QSO	z_{abs}	$\log N(\text{HI})$	$\log N(\text{SiIV})$	$\log N(\text{CIV})$	$\log N(\text{NV})$	ref
0000–263	4.06064	14.27	12.49	13.24	< 12.9	Savaglio et al. 1997
	4.06157	14.48	< 12.5	13.47	< 12.9	
	4.06248	13.19	< 12.6	13.26	< 12.9	
	4.10106	14.40	12.39	13.21	< 12.7	
	4.12605	13.76	< 12.7	13.54	< 12.8	
	4.12688	12.85	< 12.5	13.17	< 12.7	
	4.12983	15.02	< 12.5	13.46	12.66	
	4.13111	15.80	12.75	14.34	13.15	
	4.13245	15.00	12.49	14.62	13.15	
	4.13331	14.56	12.40	13.68	< 12.8	
	4.13420	15.39	12.98	14.51	13.53	
0123+257	2.3586	14.7	13.6	14.7	14.8	Barlow&Sargent 1997
	2.3618	14	–	13.7	13.65	
0424–131	2.100	15.3	12.92	13.67	< 12.7	Petitjean et al. 1994
	2.133	14.5	–	13.64	13.99	
	2.173	14.9	12.67	14.2	–	
0450–131	2.2310	14.7	13.3	13.7	14.1	
1422+231	3.5353	16.36	13.61	14.28	< 12.7	Songaila & Cowie 1996
	3.5862	15.70	12.32	13.29	< 12.3	
1946+769	3.0483	13.98	13.00	13.75	–	Fan & Tytler 1994
	3.0495	17.64	13.97	14.55	13.32	
	3.0504	14.09	13.6	14.35	12.90	
2116–358	2.30709	13.7	–	13.9	13.48	Wampler et al. 1993
	2.30680	13.3	–	14.3	14.6	
	2.30657	13.3	–	13.18	13.48	
	2.30625	13.58	–	13.85	13.3	
	2.30606	13	–	12.70	13.3	
	2.31880	14.18	13.78	15	12.9	
	2.31843	17.60	13.78	14.7	13.6	
	2.31813	14.70	13.3	14	13	
	2.31769	14.18	12.7	14.08	13.48	
	2.31702	13.9	13	13.65	13.48	

Table 9: The metal system at $z = 2.1982$.

Ion	$z = 2.198223$	
	$\log N$	b
CI	< 13.4	(25)
CIV	13.77 ± 0.05	19.8 ± 2.4
SiI	< 13.1	(25)
SiII	< 13.3	(25)
SiIV	< 13.3	(25)
AlII	< 12.3	(25)
AlIII	< 12.6	(25)
MgI	< 13.3	(25)
FeI	< 12.6	(20)
FeII	< 13.4	(20)
ZnII	< 12.7	(20)

Table 10: The metal system at $z = 2.2058$.[illegible]